UNIVERSITY OF BIRMINGHAM
University of Birmingham Research at Birmingham

Single-molecule imaging reveals receptor-G protein interactions at cell surface hot spots

Sungkaworn, Titiwat; Jobin, Marie-Lise; Burnecki, Krzysztof; Weron, Aleksander; Lohse, Martin J.; Calebiro, Davide

DOI:
10.1038/nature24264

License:
None: All rights reserved

Document Version
Peer reviewed version

Citation for published version (Harvard):
Sungkaworn, T, Jobin, M-L, Burnecki, K, Weron, A, Lohse, MJ & Calebiro, D 2017, 'Single-molecule imaging reveals receptor-G protein interactions at cell surface hot spots', *Nature*, vol. 550, pp. 543-547. https://doi.org/10.1038/nature24264

Link to publication on Research at Birmingham portal

Publisher Rights Statement:
Published in Nature, volume 550, pages 543–547 (26 October 2017)
doi:10.1038/nature24264

General rights
Unless a licence is specified above, all rights (including copyright and moral rights) in this document are retained by the authors and/or the copyright holders. The express permission of the copyright holder must be obtained for any use of this material other than for purposes permitted by law.

• Users may freely distribute the URL that is used to identify this publication.
• Users may download and/or print one copy of the publication from the University of Birmingham research portal for the purpose of private study or non-commercial research.
• User may use extracts from the document in line with the concept of 'fair dealing' under the Copyright, Designs and Patents Act 1988 (?)
• Users may not further distribute the material nor use it for the purposes of commercial gain.

Where a licence is displayed above, please note the terms and conditions of the licence govern your use of this document.

When citing, please reference the published version.

Take down policy
While the University of Birmingham exercises care and attention in making items available there are rare occasions when an item has been uploaded in error or has been deemed to be commercially or otherwise sensitive.

If you believe that this is the case for this document, please contact UBIRA@lists.bham.ac.uk providing details and we will remove access to the work immediately and investigate.

Download date: 26. Aug. 2022

1 **Single-molecule imaging reveals receptor-G protein interactions at cell surface hot spots**

2 Titiwat Sungkaworn[1,2], Marie-Lise Jobin[1,2], Krzysztof Burnecki[3], Aleksander Weron[3],

3 Martin J. Lohse[1,2,†], Davide Calebiro[1,2,4,5*]

4

5 [1]Institute of Pharmacology and Toxicology and [2]Bio-Imaging Center/Rudolf Virchow Center,
6 University of Würzburg, Germany

7 [3]Faculty of Pure and Applied Mathematics, Hugo Steinhaus Center, Wroclaw University of
8 Science and Technology, Poland

9 [4]Institute of Metabolism and Systems Research, University of Birmingham, Birmingham, UK

10 [5]Centre of Membrane Proteins and Receptors (COMPARE), Universities of Birmingham and
11 Nottingham, UK

12

13 [†]Present address: Max Delbrück Center for Molecular Medicine, Berlin, Germany

14

15 * address correspondence to:

16 Davide Calebiro, Institute of Pharmacology and Toxicology, Versbacher Str. 9,

17 97078 Würzburg, Germany – E-mail: davide.calebiro@toxi.uni-wuerzburg.de

18

G protein-coupled receptors (GPCRs) mediate the biological effects of many hormones and neurotransmitters and are major pharmacological targets[1]. They transmit their signals to the cell interior via interaction with G proteins. However, how receptors and G proteins meet, interact and couple is still ill understood. Here, we analyse the concerted motion of GPCRs and G proteins on the plasma membrane and provide a quantitative model that reveals the key factors at the basis of the high spatiotemporal complexity of their interactions. Using two-colour, single-molecule imaging we visualize interactions between individual receptors and G proteins at the surface of living cells. Under basal conditions, receptors and G proteins form activity-dependent complexes that last for ~1 second. Different agonists specifically regulate the kinetics of receptor-G protein interactions, mostly increasing their association rate. We find hot spots on the plasma membrane, at least partially defined by the cytoskeleton and clathrin-coated pits, where receptors and G proteins are confined and preferentially couple. Imaging with the nanobody Nb37 suggests that signalling preferentially occurs at these hot spots. These findings shed new light on the dynamic interactions governing GPCR signalling.

Different scenarios have been developed to explain how receptors and G proteins interact[2,3]. However, key questions concerning the stability of these interactions and the occurrence of GPCR signalling subdomains at the plasma membrane are still open (see also Supplementary Discussion). To address these questions, we visualized individual receptors and G proteins at the surface of living cells with high spatial (≈20 nm) and temporal (≈30 ms) resolution[4]. As a model, we chose the α_{2A}-adrenergic receptor (α_{2A}-AR), a prototypical family-A GPCR with strong G_i coupling[2]. The α_{2A}-AR and a pertussis toxin (PTX)-insensitive $G\alpha_{i1}$ construct were specifically labelled with two different organic fluorophores via a SNAP[5] or CLIP[6] tag, respectively (Fig. 1a); both constructs were fully functional (Extended Data Fig. 1a, b). These constructs were transiently expressed at low physiological densities (0.55±0.10 and 0.51±0.09 molecule μm^{-2}, respectively) in CHO cells – cultured with PTX to inactivate endogenous $G_{i/o}$ proteins – and simultaneously imaged by fast two-colour single-molecule microscopy combined with single-particle tracking[4] (Fig. 1b and Supplementary Videos 1 and 2). Labelling efficiencies were ~90% (extracellular) and ~80% (intracellular); non-specific labelling was <1% (Extended Data Fig. 1c-e).

Individual α_{2A}-AR trajectories were evaluated by mean square displacement (MSD) analysis (corrected for localization error, see Supplementary Methods), which revealed a high heterogeneity and features of anomalous diffusion[7]. Under basal conditions, 11% of the receptors were virtually immobile, while 38% had sub-, 45% normal and 6% super-diffusion (i.e. directional motion) (Extended Data Fig. 2). $G\alpha_i$ had a significantly different diffusion pattern, with a larger immobile fraction (37%) (Extended Data Fig. 2c, d). Stimulation with the full agonist norepinephrine (NE) or brimonidine (UK-14,304) caused a small, significant change in the overall diffusion pattern of $G\alpha_i$ but not of α_{2A}-AR (Extended Data Fig. 2d). Similar results were obtained for a second receptor/G protein pair, i.e. β_2-adrenergic receptor (β_2-AR) and $G\alpha_s$, but no significant differences were observed upon stimulation with the full agonist isoproterenol (Iso; Extended Data Fig. 2d).

We then analysed the trajectories with an algorithm based on hidden Markov models (HMMs)[8], which assumes that particles switch among discrete diffusive states following a stochastic process. We found that both receptors and G proteins frequently switched among at least four distinguishable states (S1 to S4), characterized by distinct diffusion coefficients (*D*) and ranging from a virtually immobile (S1) to a fast diffusive (S4) state (Fig. 1c-f and Extended Data Fig. 3). The results were overall consistent with those of the MSD analysis. We hypothesized that the two slowest states (S1 and S2) were due to trapping in small membrane compartments and, based on the corresponding *D* and average dwell times, we estimated compartment radiuses of <50 nm and ~270 nm, respectively (see Supplementary Methods). Although with some differences, a similar picture was observed for the integral membrane protein CD86 – used as control[4] (Fig. 1f, Extended Data Figs. 2d and 3), indicating that such diffusion behaviour is not unique to GPCRs/G proteins.

Density maps of single-molecule localizations revealed areas that were either preferentially explored or avoided by α_{2A}-ARs and $G\alpha_i$ subunits (Extended Data Fig. 4a and Supplementary Video 3). To better characterize these areas, we generate dynamic maps from the trajectories, reporting local *D* and potential energy (*V*) values[9]. This analysis revealed a complex dynamic landscape at the plasma membrane, with high-potential areas, which were rapidly left by α_{2A}-ARs/$G\alpha_i$ subunits, and low-potential areas, where they tended to be trapped (Extended Data Fig. 4b, dark areas; see Extended Data Fig. 1f for control). There was a partial but consistent overlap between the potential energy maps of α_{2A}-ARs and $G\alpha_i$ subunits (Extended Data Fig. 4c). To quantify this, we measured the relative potential energy values ($V_{L,rel}$) of $G\alpha_i$ at the sites of α_{2A}-AR localization and vice versa, which were both significantly lower than for random

localizations or compared to CD86 (Fig. 2a). Importantly, receptor:G protein interactions preferentially occurred at the shared low potential energy areas ("hot spots"), as indicated by negative $V_{L,rel}$ values (Fig. 2b). Similar results were obtained for β_2-AR and $G\alpha_s$ (Extended Data Fig. 5a, b).

To investigate possible factors responsible for this complex diffusion dynamics, we imaged both the cytoskeleton and clathrin-coated pits (CCPs) underneath the plasma membrane. α_{2A}-ARs trajectories tended to avoid microtubules and actin fibres, as suggested by negative colocalization index values (Fig 2c, d, Supplementary Videos 4 and 5), in agreement with the fence-and-picket model[10]. Moreover, the majority of trajectories tended to avoid CCPs (Fig. 2e, Supplementary Video 6). This coexisted with a minor fraction of α_{2A}-ARs that either transiently stopped at CCPs (Fig. 2f, arrowheads) – consistent with receptor recruitment to pre-existing CCPs[11] – or were immobile and localized at CCPs. The fraction of CCPs occupied by α_{2A}-ARs increased upon agonist stimulation (Fig. 2f, right), Overlays of single particle trajectories with superresolved actin images, obtained by photoactivated localization microscopy (PALM)[12], suggested that the actin mesh underneath the plasma membrane created sub-micrometre compartments in which α_{2A}-ARs were apparently loosely trapped (Fig. 2g and Supplementary Video 7; radius ~100-300 nm, in agreement with estimation based on HMM analysis). Consistently, superimposition of PALM images with potential energy maps showed that the low potential areas were often at least partially delimited by actin fibres (Fig. 2h and Extended Data Fig. 4d). Similar results were obtained for β_2-AR (Extended Data Fig. 5c-f) and $G\alpha_i$ (Extended Data Fig. 6 and Supplementary Video 8).

Next, we developed a mathematical analysis to estimate the duration of receptor:G protein interactions based on their trajectories. We reasoned that, on average, for two particles undergoing a true interaction, their observed colocalization time (Δt_{obs}) should correspond to the average duration of true interactions (Δt_{true}) plus the average duration of random colocalizations (Δt_{random}) (Fig. 3a and Extended Data Fig. 7). Thus, we deconvolved the observed colocalization times with those of random colocalizations (obtained with CD86 and $G\alpha_i$) to estimate the distribution of the underlying true receptor:G protein interactions (Fig. 3b and Supplementary Methods). The results were subsequently expressed as normalized relaxation curves, showing the fraction of the interactions that are still ongoing at time t from the beginning of each interaction (Fig. 3c). The very fast component in Fig. 3b, seen also with the control CD86, corresponds to non-productive interactions plus random colocalizations, the rate of which (k_{np+rc}) did not differ among the conditions tested (Fig. 3d, left), while we considered the remainder to

117 be productive interactions, i.e. interactions that result in the formation of a "true" complex (see
118 Supplementary Discussion). α_{2A}-ARs and $G\alpha_i$ underwent some productive interactions already
119 under basal conditions (Fig. 3b, c). A major fraction of these interactions terminated following an
120 exponential decay, while a very small fraction (approximately $3 \cdot 10^{-4}$) was stable over the
121 observation time (Fig. 3c). From a fitting of the major component in Fig. 3c and the particle
122 densities we estimated an association rate constant (k_{on}) of ~0.015 μm^2 molecule^{-1} s^{-1} and a
123 dissociation rate constant (k_{off}) of ~0.8 s^{-1} for the productive interactions under basal conditions
124 (Fig. 3d, middle/right). Treatment with an inverse agonist (yohimbine) or $G\alpha_i$ inactivation (using
125 a PTX-sensitive construct) suppressed the major fraction of transient productive interactions,
126 suggesting that they resulted from constitutive α_{2A}-AR activity and required a functional $G\alpha_i$
127 subunit; in contrast, the small fraction of stable productive interactions was not affected (Fig.
128 3e). Stimulation with norepinephrine caused a concentration-dependent increase of k_{on} up to
129 ~0.2 μm^2 molecule^{-1} s^{-1}, while k_{off} was only marginally affected (Fig. 3b-d). This translates into 2-
130 dimensional equilibrium dissociation constants (K_d) of ~50 and 6 molecule μm^{-2} for basal and
131 stimulated conditions, respectively. Based on these results, we estimated that, at the tested
132 densities, ~0.5% (basal) or 5% (stimulated) of all α_{2A}-ARs were in complex with $G\alpha_i$ at any given
133 time. Similar results were obtained for β_2-AR:$G\alpha_s$ interactions, although with 10-fold lower k_{on}
134 values and no long-lived interactions (Fig. 3f, g). A panel of α_{2A}-AR agonists with varying
135 efficacy and affinity revealed statistically significant differences in the estimated k_{on} and, to a
136 lesser extent, k_{off} values (Fig. 3d). Overall, there was a positive correlation between k_{on} and
137 efficacy (Fig. 3h). However, there was also a trend towards smaller k_{on} values for higher affinity
138 agonists, both considering full (UK-14,304 vs. norepinephrine) or partial (clonidine vs.
139 oxymetazoline) agonists with comparable efficacies and dissimilar affinities (Fig. 3d, h).

140 By visually inspecting the trajectories, we observed that several α_{2A}-ARs and $G\alpha_i$ subunits
141 slowed down or stopped during apparent interactions to then either remain confined or resume
142 their motion (Fig. 3i, Fig 3j, left and Supplementary Video 9), while the remainder retained their
143 mobility (Fig. 3j, right). A quantitative analysis of the HMM states of α_{2A}-AR and $G\alpha_i$ trajectories
144 showed that, during the time of interaction, higher fractions of receptors/G proteins were in
145 states S1 (virtually immobile) and S2 (slowly diffusing) (Fig. 3k). These mobility changes
146 occurring during the short interaction times and the global changes in $G\alpha_i$ diffusion described in
147 Extended Data Fig. 2d and 3 likely represent distinct phenomena.

148 To further validate our results, we performed deterministic simulations of GPCR signalling using
149 the estimated microscopic k_{on} and k_{off} values for receptor:G protein interactions. The results

150 were in very good agreement with ensemble (FRET) measurements of α_{2A}-AR/G_i
151 association/dissociation (Extended Data Fig. 8). These simulations also suggested that G
152 protein signalling can be fast only if it occurs while the G protein is still bound to the receptor
153 (Supplementary Data). Moreover, we performed particle-based stochastic simulations of
154 receptors and G proteins diffusing and interacting on a 2D surface (Fig 4a). Introducing the
155 experimentally measured potential energy (*V*) landscapes (as in Fig. 2b) in these simulations
156 doubled the probability of receptor:G protein interactions compared to conditions of simple
157 Brownian motion (Fig. 4a).

158 To investigate whether hot spots for receptor:G protein interactions also occur in a more
159 physiological context, we studied primary human endothelial cells (HUVEC), where both α_{2A}-
160 and β_2-ARs are endogenously expressed and regulate vascular tone[13]. We found that in these
161 cells both α_{2A}-AR:Gα_i and β_2-AR:Gα_s interactions were preferentially occurring at low potential
162 energy areas (Extended Data Fig. 9a, b). We also found that receptors and G proteins slowed
163 down or stopped moving during their interactions (Extended Data Fig. 9c), further strengthening
164 our observations in CHO cells.

165 Finally, we assessed G_s activation using the conformation-sensitive nanobody Nb37[14,15], which
166 recognizes the active (nucleotide-free) state of Gα_s. In HUVEC transfected with Nb37 fused to a
167 fluorescent protein (EYFP), Nb37 preferentially localized at the sites where β_2-ARs were
168 concentrated (Fig. 4b).

169 The main findings of our study are summarized in Extended Data Figure 10. First, our results
170 reveal a complex picture, whereby barriers, at least partially constituted by actin fibres,
171 microtubules and CCPs, contribute to the formation of hot spots where receptors and G proteins
172 are both concentrated, and where G protein coupling as well as signalling preferentially occur.
173 This provides a direct visualization of previously postulated GPCR signalling nanodomains[16,17].
174 Based on our results and simulations, we hypothesize that this complex organization increases
175 both the speed and efficiency of receptor:G protein coupling, while allowing G protein signalling
176 to occur locally.

177 Second, our data provide direct estimates of the frequency and duration of receptor:G protein
178 interactions in living cells. We find that most receptor:G protein interactions are short-lived
179 (lifetime ~1-2 s). The dependency of these complexes on receptor activation suggests that they
180 are linked to signalling, which is further supported by the observation that G protein activation
181 occurs preferentially at the sites of interaction. In addition, we observe a very small fraction of

long-lived complexes (lifetime >> 4s), possibly corresponding to those reported in previous studies[3,18]. The coexistence of short- and long-lived complexes might reconcile earlier contrasting data. Intriguingly, the estimated duration of the short-lived interactions is much longer than the time required for effector activation, which can happen in ~40 ms[2]. Thus, as suggested by our deterministic simulations, it is conceivable that fast effector activation might occur while the G protein is still bound to the receptor[19].

Third, our results reveal that receptor:G protein interactions are regulated by agonists largely at the level of k_{on}. The low k_{on} values measured here also indicate that random collisions only seldom lead to the formation of productive receptor:G protein complexes. The fact that k_{on} is regulated by agonists and the low k_{on} values suggest that receptor:G protein interactions are not limited by diffusion, but rather by the major conformational changes occurring during the formation of receptor:G protein complexes[14,20-22] (see also Supplementary Discussion). Interestingly, different agonists induce substantially different k_{on} values, which correlate at least partially with their efficacies. Together with small differences in the k_{off} values, these findings suggest the possibility of fine-tuning receptor signalling using drugs with tailored effects on the kinetics of receptor:G protein interactions. Finally, our finding of lower k_{on} values for β_2-AR:Gα_s than for α_{2A}-AR:Gα_i interactions is consistent with the view that coupling to G_s might require a larger conformational change than coupling to G_i[23].

In summary, our single-molecule results reveal new key factors involved in the regulation of receptor:G protein interactions, which may allow modifying receptor signalling in ways that far exceed simple receptor blockade or activation achieved with currently available drugs, for example by modulating the on/off rates of receptor:G protein interactions or manipulating receptor/G protein mobility and coupling at the hot spots. They further illustrate how GPCR signalling results from dynamic interactions among receptors, G proteins and the complex surrounding membrane environment, which confers flexibility and versatility to this fundamental biological process.

References

1 Pierce, K. L., Premont, R. T. & Lefkowitz, R. J. Seven-transmembrane receptors. *Nat. Rev. Mol. Cell. Biol.* **3**, 639-650 (2002).

2 Hein, P., Frank, M., Hoffmann, C., Lohse, M. J. & Bünemann, M. Dynamics of receptor/G protein coupling in living cells. *EMBO J.* **24**, 4106-4114 (2005).

214 3 Galès, C. *et al.* Probing the activation-promoted structural rearrangements in preassembled
215 receptor-G protein complexes. *Nat. Struct. Mol. Biol.* **13**, 778-786 (2006).

216 4 Calebiro, D. *et al.* Single-molecule analysis of fluorescently labeled G-protein-coupled
217 receptors reveals complexes with distinct dynamics and organization. *Proc. Natl. Acad. Sci.*
218 *U. S. A.* **110**, 743-748 (2013).

219 5 Keppler, A. *et al.* A general method for the covalent labeling of fusion proteins with small
220 molecules in vivo. *Nat. Biotechnol.* **21**, 86-89 (2003).

221 6 Gautier, A. *et al.* An engineered protein tag for multiprotein labeling in living cells. *Chem.*
222 *Biol.* **15**, 128-136 (2008).

223 7 Magdziarz, M., Weron, A., Burnecki, K. & Klafter, J. Fractional Brownian motion versus the
224 continuous-time random walk: a simple test for subdiffusive dynamics. *Phys. Rev. Lett.* **103**,
225 180602 (2009).

226 8 Persson, F., Linden, M., Unoson, C. & Elf, J. Extracting intracellular diffusive states and
227 transition rates from single-molecule tracking data. *Nat. Methods* **10**, 265-269 (2013).

228 9 El Beheiry, M., Dahan, M. & Masson, J.-B. InferenceMAP: mapping of single-molecule
229 dynamics with Bayesian inference. *Nat. Methods* **12**, 594-595 (2015).

230 10 Kusumi, A., Shirai, Y. M., Koyama-Honda, I., Suzuki, K. G. & Fujiwara, T. K. Hierarchical
231 organization of the plasma membrane: investigations by single-molecule tracking vs.
232 fluorescence correlation spectroscopy. *FEBS Lett.* **584**, 1814-1823 (2010).

233 11 Scott, M. G., Benmerah, A., Muntaner, O. & Marullo, S. Recruitment of activated G protein-
234 coupled receptors to pre-existing clathrin-coated pits in living cells. *J. Biol. Chem.* **277**,
235 3552-3559 (2002).

236 12 Betzig, E. *et al.* Imaging intracellular fluorescent proteins at nanometer resolution. *Science*
237 **313**, 1642-1645 (2006).

238 13 Vanhoutte, P. M. Endothelial adrenoceptors. *J. Cardiovasc. Pharmacol.* **38**, 796-808 (2001).

239 14 Rasmussen, S. G. *et al.* Crystal structure of the β_2 adrenergic receptor-G_s protein complex.
240 *Nature* **477**, 549-555 (2011).

241 15 Irannejad, R. *et al.* Conformational biosensors reveal GPCR signalling from endosomes.
242 *Nature* **495**, 534-538 (2013).

243 16 Insel, P. A. *et al.* Compartmentation of G-protein-coupled receptors and their signalling

244 components in lipid rafts and caveolae. *Biochem. Soc. Trans.* **33**, 1131-1134 (2005).

245 17 Pontier, S. M. *et al.* Cholesterol-dependent separation of the β_2-adrenergic receptor from its
246 partners determines signaling efficacy: insight into nanoscale organization of signal
247 transduction. *J. Biol. Chem.* **283**, 24659-24672 (2008).

248 18 Qin, K., Dong, C., Wu, G. & Lambert, N. A. Inactive-state preassembly of G_q-coupled
249 receptors and G_q heterotrimers. *Nat. Chem. Biol.* **7**, 740-747 (2011).

250 19 Rebois, R. V. *et al.* Heterotrimeric G proteins form stable complexes with adenylyl cyclase
251 and Kir3.1 channels in living cells. *J. Cell. Sci.* **119**, 2807-2818 (2006).

252 20 Westfield, G. H. *et al.* Structural flexibility of the $G\alpha_s$ α-helical domain in the β_2-adrenoceptor
253 G_s complex. *Proc. Natl. Acad. Sci. U. S. A.* **108**, 16086-16091 (2011).

254 21 Dror, R. O. *et al.* Structural basis for nucleotide exchange in heterotrimeric G proteins.
255 *Science* **348**, 1361-1365 (2015).

256 22 Gregorio, G. G. *et al.* Single-molecule analysis of ligand efficacy in β_2AR–G-protein
257 activation. *Nature* **547**, 68-73 (2017).

258 23 Rose, A. S. *et al.* Position of transmembrane helix 6 determines receptor G protein coupling
259 specificity. *J. Am. Chem. Soc.* **136**, 11244-11247 (2014).

260 24 Nikolaev, V. O., Hoffmann, C., Bunemann, M., Lohse, M. J. & Vilardaga, J. P. Molecular
261 basis of partial agonism at the neurotransmitter α_{2A}-adrenergic receptor and G_i-protein
262 heterotrimer. *J. Biol. Chem.* **281**, 24506-24511 (2006).

263

264 **Supplementary Information** is linked to the online version of the paper at
265 www.nature.com/nature.

266

267 **Acknowledgements** We thank Steve P. Watson, Markus Sauer, Carlo Manzo and Emanuele
268 Cocucci for helpful discussions. This work was supported by a grant of the Deutsche
269 Forschungsgemeinschaft (Sonderforschungsbereich/Transregio 166–Project C1 to D.C.) and in
270 part by funds of the Deutsche Forschungsgemeinschaft (grant CA 1014/1-1 to D.C. and FZT82
271 Rudolf Virchow Center to M.J.L.), the IZKF Würzburg (grant B-281 to D.C.), the European
272 Research Council (Advanced Grant 232944–TOPAS to M.J.L.) and the Polish National Science
273 Center (Maestro Grant No. 2012/06/A/ST1/00258 to K.B. and A.W.). T.S. was in part supported

274 by an Alexander-von-Humboldt/Bayer Foundation fellowship.

275

276 **Author contributions** T.S. and M-L.J. performed the experiments. T.S., M-L.J., K.B. and D.C.
277 analysed the data. K.B., A.W. and D.C. developed the mathematical analyses. D.C. wrote the
278 software. D.C. and T.S. wrote the manuscript with contribution of M.J.L. All authors discussed
279 the results. D.C. conceived and supervised the study.

280

281 **Author information** Reprints and permissions information is available at
282 www.nature.com/reprints. The authors declare no competing financial interests.
283 Correspondence and requests for materials should be addressed to D.C.
284 (davide.calebiro@toxi.uni-wuerzburg.de).

285

286 **Figure Legends**

287 **Figure 1 | Single-molecule imaging of receptors/G proteins. a,** Overall strategy. The α_{2A}-AR
288 was labelled with S549-BG via a SNAP tag fused to its N-terminus. The G_i protein was labelled
289 with SiR-BC via a CLIP tag inserted in an internal loop of the $G\alpha_i$ subunit. **b**, Selected frame
290 from a fast single-molecule image sequence (left) and corresponding trajectories (right). **c-e,**
291 HMM analysis of diffusive states. Shown is a representative α_{2A}-AR trajectory (**c**), with its
292 displacement (*r*) over time (**d**) and the result of the global HMM analysis (**e**) revealing 4 states
293 (S1-S4, labelled with different colours). **f,** Model and diffusion coefficients (*D;* μm^2 s^{-1}) derived
294 from the HMM analysis. Each state is represented by a solid circle; circle area and arrow
295 thickness proportional to occupancy and transition probability, respectively. Differences were
296 statistically significant by two-way ANOVA. *, $P<0.05$, **, $P<0.01$, ***, $P<0.001$, ****, $P<0.0001$
297 vs. corresponding state of α_{2A}-AR by Tukey's multiple comparison test. Data are mean±s.d.
298 n=22 (85,475), 13 (47,062) and 28 (110,907) cells (trajectories) for α_{2A}-AR, $G\alpha_i$ and CD86,
299 respectively. Images (**b**, **c**) represent 5 independent experiments.

300

301 **Figure 2 | Complex diffusion dynamics generates hot spots for receptor:G protein**
302 **interactions. a,** α_{2A}-AR localizations over $G\alpha_i$ potential energy map (left) and quantifications of
303 relative potential energy at the localizations ($V_{L,rel}$; right). **b**, α_{2A}-AR:$G\alpha_i$ interactions over merged
304 α_{2A}-AR and $G\alpha_i$ potential energy (*V*) maps (left) and corresponding quantifications (right).

305 Arrowheads, localizations concentrated at hot spots. **c-e,** α_{2A}-AR trajectories over images of
306 tubulin (**c**), actin (**d**) or CCPs (**e**) (left) and corresponding colocalization analyses (right). **f**,
307 Trajectories of α_{2A}-ARs (colour-coded according to HMM states) stopping at CCPs (arrowheads;
308 left) and corresponding quantitative analysis (right). **g**, α_{2A}-AR trajectories over actin PALM
309 image (left) and corresponding colocalization analysis (right). Arrowheads, α_{2A}-ARs crossing
310 over actin fibres. **h,** α_{2A}-AR potential energy map over actin PALM image (left) and zoom-in view
311 showing hot spot surrounded by actin fibres (right). α_{2A}-ARs in **g** and **h** were labelled with S647-
312 BG. Results (**a-e**, **g**) were compared to random localizations. See Supplementary Methods for
313 details. Data are mean±s.d. n, number of cells. #, P<0.05, ##, P<0.01, ###, P<0.001, ####,
314 P<0.0001 vs. random localizations by two-sided paired t-test. *, P<0.05, ****, P<0.0001 vs. α_{2A}-
315 AR (basal) by two-sided unpaired t-test. Images (**h**) represent 2 independent experiments.

316

317 **Figure 3 | Analysis of receptor:G protein interactions. a,** Schematic comparison between
318 random colocalizations and true interactions. On average, the observed duration of true
319 interactions (Δt_{obs}) corresponds to their true duration (Δt_{true}) plus that of random colocalizations
320 (Δt_{random}). The distribution of true durations can then be estimated via deconvolution. **b,**
321 Distributions of the estimated durations of α_{2A}-AR:Gα_i interactions under basal and stimulated
322 (NE, 100 μM) conditions, based on deconvolution. CD86 was used as non-interacting control. **c,**
323 Relaxation curves calculated from the data in **b**, showing the dissociation kinetics of α_{2A}-AR:Gα_i
324 complexes (left, linear; right, semilogarithmic plot). **d,** Estimated rate constants of non-
325 productive interactions plus random colocalizations (k_{np+rc}; left), α_{2A}-AR:Gα_i association ($k_{on;}$
326 middle) and dissociation (k_{off}; mean, 95%CI; right) for the indicated ligands. Differences in k_{on}
327 values are statistically significant by one-way ANOVA. ****, P<0.0001 vs. NE 100 μM by Tukey's
328 multiple comparison test. Differences in k_{off} values vs. NE 100 μM were assessed by two-sided
329 unpaired t-test with Bonferroni correction (****, P<0.0001). **e**, Relaxation curves of α_{2A}-AR:Gα_i
330 interactions obtained with an inverse agonist (yohimbine) or using a PTX-sensitive Gα_i
331 construct. **f**, Relaxation curves of β_2-AR:Gα_s interactions. **g,** Estimated k_{on} and k_{off} (mean,
332 95%CI) for β_2-AR:Gα_s interactions. ****, P<0.0001 vs. Iso by two-sided unpaired t-test. **h,**
333 Relationship between measured k_{on} and efficacy on α_{2A}-AR activation (mean±s.e.m.). Brackets,
334 affinity values (pK_i). Efficacy and affinity values are from ref. 24. **i,** Apparent interaction between
335 α_{2A}-AR and Gα_i lasting for 1.2 s. After the interaction, the receptor resumes moving, whereas
336 the G protein remains immobile. **j,** α_{2A}-AR and Gα_i trajectories stopping (left) or continuing

337 moving (right) during apparent interactions. **k,** Distribution of diffusive states (based on HMM
338 analysis) of α_{2A}-AR and $G\alpha_i$ (NE, 100 μM) during apparent interactions (colocalization duration ≥
339 1.1 s) compared to time outside interactions. Differences are statistically significant by chi-
340 square test (****, P<0.0001; n=1,265,634 and 527,058 data points for α_{2A}-AR and $G\alpha_i$,
341 respectively). All ligands were used at saturating concentrations, unless otherwise indicated.
342 See Supplementary Methods for details. Data are mean±s.d., unless otherwise indicated. n,
343 number of cells (**d**, **g**). Images (**i, j**) represent 5 independent experiments. N.D., not
344 determinable.

345

346 **Figure 4 | Hot spots for receptor-G protein signalling. a,** Stochastic simulations of
347 receptor:G protein interactions. Left, simulated trajectories. Right, fraction of interacting
348 molecules over time. Compared are results with experimentally measured potential energy (*V*)
349 landscapes vs. simple Brownian motion. **b**, Visualization of local G_s protein activation at the
350 plasma membrane of primary human endothelial cells. Cells were transfected with a fluorescent
351 sensor (Nb37-EYFP) recognizing active, nucleotide-free $G\alpha_s$. Left, β_2-AR localizations over the
352 obtained spatial map of G_s protein activity. Right, quantification. Data are mean±s.d. n, number
353 of cells. ####, P<0.0001 vs. random localizations by two-sided paired t-test.

354

355 **Methods**

356 **Materials**

357 Cell culture reagents, Lipofectamine 2000, Lipofectamine 3000, TetraSpeck fluorescent beads,
358 fluorescein arsenical hairpin binder (FlAsH) and CellMask Green Plasma Membrane Stain were
359 from Thermo Fisher Scientific. The Effectene transfection reagent was from Qiagen. UK-14,304
360 and clonidine were from Tocris Bioscience. All other GPCR ligands, pertussis toxin (PTX), 1,2-
361 ethanedithiol (EDT) and guanosine 5′-triphosphate (GTP) were from Sigma-Aldrich. [^{35}S]GTPγS
362 was from PerkinElmer. The fluorescent benzyl guanine derivatives SNAP-Surface 549 (S549-
363 BG) and SNAP-Surface Alexa Fluor 647 (S647-BG) were from New England Biolabs. Live-cell
364 fluorogenic probes for actin (SiR-Actin) and tubulin (SiR-Tubulin)[25] were from Spirochrome. The
365 silicon-rhodamine benzyl cytosine derivative (SiR-BC)[26] was kindly provided by Kai Johnsson
366 (Max Planck Institute for Medical Research, Heidelberg, Germany). Ultraclean glass coverslips
367 were obtained as previously described[4].

368

369 **Molecular biology**

370 A plasmid coding for the N-terminally SNAP-tagged α_{2A}-adrenergic receptor (SNAP-α_{2A}-AR)
371 was generated by inserting the SNAP tag[5] before the coding sequence of the murine α_{2A}-
372 adrenergic receptor. The generation and functional characterization of the N-terminally SNAP-
373 tagged β_2-adrenergic receptor construct (SNAP-β_2-AR) have been described in a previous
374 study[4]. A plasmid ($G\alpha_i$-CLIP) coding for the rat $G\alpha_{i1}$ subunit with the CLIP tag[6] inserted in the
375 αA-αB loop within the α-helical domain (between positions 91 and 92) was generated by
376 replacing YFP with the CLIP tag in a previously described YFP-tagged $G\alpha_{i1}$ construct[27]. The
377 construct additionally harboured the C351I mutation to render it PTX-insensitive[28]. A plasmid
378 coding for the rat $G\alpha_s$ subunit with the CLIP tag inserted between positions 72 and 85 ($G\alpha_s$-
379 CLIP) was generated by replacing YFP with the CLIP tag in a previously described YFP-tagged
380 $G\alpha_s$ construct[29]. All tagged receptor and $G\alpha$ subunit constructs behaved like the corresponding
381 wild type in functional assays (Extended Data Fig. 1a, b). A construct coding for His-tagged
382 Nb37[14] was kindly provided by Jan Steyaert (VIB, Brussels, Belgium). A plasmid coding for the
383 C-terminally EYFP-tagged Nb37 (Nb37-EYFP) was generated by fusing EYFP to the C-terminus
384 of Nb37. Plasmids coding for CD86 with either one or two SNAP tags fused to its N-terminus
385 have been previously described[4]. Plasmids coding for CD86 with either one or two CLIP tags
386 fused to its C-terminus were generated by inserting either one or two copies of the CLIP tag
387 before the stop codon of CD86.

388

389 **Cell culture and transfection**

390 Chinese hamster ovary K1 (CHO-K1) cells (ATCC) were cultured in phenol red-free Dulbecco's
391 modified Eagle's medium (DMEM)/F-12 supplemented with 5% FCS, 100 U/ml penicillin and 0.1
392 mg/ml streptomycin at 37 °C, 5% CO_2. For single-molecule experiments, CHO-K1 cells were
393 seeded on ultraclean 24-mm glass coverslips in 6-well culture plates at a density of $3 \cdot 10^5$
394 cells/well. Cells were treated with 50 ng/ml pertussis toxin (PTX) to inactivate endogenous $G\alpha_{i/o}$
395 proteins. Transfection was performed 24 h after seeding using Lipofectamine 2000. For each
396 well, 0.8 µg SNAP-α_{2A}-AR or SNAP-β_2-AR, 0.6 µg $G\alpha_i$-CLIP or $G\alpha_s$-CLIP, 0.4 µg $G\beta_1$, 0.2 µg
397 $G\gamma_2$, and 6 µL Lipofectamine 2000 were used. Cells were labelled and imaged by single-
398 molecule microscopy 4-6 h after transfection to obtain low physiological expression levels[4]. To
399 label CCPs, cells were transfected 24 h prior to the experiment with GFP-tagged adaptor protein
400 2 (AP2-GFP), kindly provided by Tom Kirchhausen (Harvard Medical School, USA). Human

401 embryonic kidney 293 (HEK293) cells (ATCC) were cultured in DMEM supplemented with 5%
402 FCS, 100 U/ml penicillin and 0.1 mg/ml streptomycin at 37 °C, 5% CO_2. HEK293 cells were
403 transfected with Effectene, following the manufacturer's instructions. Cell lines have not been
404 authenticated. Cells were routinely tested for mycoplasma contamination by PCR using specific
405 primers.

406 For the [^{35}S]GTPγS binding experiments, HEK293 cells were plated in 10-cm culture dishes and
407 transfected with 3.3 μg α_{2A}-AR, 3.3 μg wild-type or CLIP tagged Gα_i, 2.0 μg Gβ_1 and 1.5 μg Gγ_2
408 plasmids.

409 For FRET experiments, HEK293 cells were seeded on poly-L-lysine–coated 24-mm coverslips
410 and transfected with the indicated constructs. The α_{2A}-AR-Flash/CFP sensor was used to
411 monitor receptor activation[30]. Co-transfection of α_{2A}-AR-YFP, Gα_i-CFP, Gβ_1 and Gγ_2 was used to
412 monitor G protein recruitment to the receptor[2]. The Gβ_1-2A-cpV-Gγ_2-IRES-Gα_{i2}-mTq2 sensor[31]
413 was used to monitor G_i protein activation.

414 Human umbilical vein endothelial cells (HUVEC) were purchased from Lonza and cultured in
415 complete EGM-2 BulletKit medium (Lonza). HUVEC were plated on ultraclean 24-mm glass
416 coverslips at a density of $3.5 \cdot 10^5$ cells/well and transfected with Lipofectamine 3000 using the
417 same DNA amounts indicated for CHO cells. HUVEC were cultured for a maximum of 10
418 passages. To visualize local G_s protein activation at the plasma membrane, HUVEC were
419 transfected 24 h prior to the experiment with the Nb37-EYFP construct.

420

421 **[^{35}S]GTPγS binding assay**

422 Membrane preparation and [^{35}S]GTPγS binding assay were performed following a previously
423 described protocol[32]. Cells were homogenized in lysis buffer (5 mM Tris, 2 mM EDTA, pH 7.4)
424 and then centrifuged at 1,000xg for 10 min. The supernatant was collected and centrifuged at
425 50,000xg for 30 min. The remaining pellet was resuspended in binding buffer (100 mM NaCl, 10
426 mM $MgCl_2$, 20 mM HEPES, pH 7.4). All procedures were performed at 4 °C. Protein
427 concentrations were determined using the Bradford assay. 10 μg membrane proteins were then
428 incubated with the indicated agonist concentrations and 100 pM [^{35}S]GTPγS for 15-300 s. Non-
429 specific binding was evaluated by adding 10 μM GTP. The samples were then passed through
430 glass fibre filters and radioactivity was determined using a liquid scintillation counter (Beckman
431 LS-1801).

432

433 **Live-cell protein labelling**

434 Cells were labelled with a combination of a cell-impermeable SNAP substrate (S549-BG), to
435 label cell-surface receptors, and a highly cell-permeable CLIP substrate (SiR-BC)[26], to label
436 intracellular G proteins. Cells were incubated with 4 μM S549-BG and 8 μM SiR-BC in complete
437 culture medium for 20 min at 37 °C. Cells were then washed three times using complete culture
438 medium, with 5 min incubation after each wash. This protocol gives labelling efficacy of ~90%
439 and ~80% for extracellular SNAP and intracellular CLIP labelling, respectively (Extended Data
440 Fig. 1c, d).

441 Actin and tubulin labelling were performed using SiR-actin and SiR-tubulin, respectively,
442 following the manufacturer's protocol. Briefly, cells were labelled with 3 μM SiR-actin or SiR-
443 tubulin in the presence of 10 μM verapamil for 20 min at 37 °C, followed by three washes with
444 complete culture medium.

445 FlAsH labelling was performed as previously described[30]. Briefly, cells were incubated with 1 μM
446 FlAsH and 12.5 μM EDT in Hank's balanced salt solution (HBSS) for 1 h. The cells were then
447 washed twice with HBSS and incubated with 250 μM EDT in HBSS for 10 min. The cells were
448 washed a third time with HBSS immediately before the FRET measurement.

449

450 **FRET measurements**

451 Fluorescence resonance energy transfer (FRET) experiments to examine the ensemble kinetics
452 of receptor/G protein signalling in intact cells were done as previously described[2,33,34].
453 Measurements were performed on an Axiovert 200 inverted microscope (Zeiss) equipped with
454 an oil immersion 100X objective (Plan-Neofluar 100x, N.A. 1.30), a beamsplitter (DCLP505) and
455 a Polychrome IV monochromator and dual-emission photometric system (Till Photonics).
456 Transfected HEK293 cells were placed in a microscopy chamber filled with imaging buffer (137
457 mM NaCl, 5.4 mM KCl, 2 mM $CaCl_2$, 1 mM $MgCl_2$, 10 mM HEPES, pH 7.3). Agonist stimulation
458 was applied using a pressurized rapid superfusion system (ALA-VM8, ALA Scientific
459 Instruments). FRET was monitored as the ratio between YFP (535±15 nm) and CFP (480±20)
460 emission upon CFP excitation at 436±10 nm. The YFP signal was corrected for direct excitation
461 and bleed-through of CFP emission into the YFP channel as previously described[2].

462

463 **Single-molecule microscopy and PALM**

464 Single-molecule microscopy experiments were performed using total internal reflection
465 fluorescence (TIRF) illumination on a custom Nikon Eclipse Ti TIRF microscope equipped with
466 405 nm, 488 nm, 561 nm and 640 nm diode lasers (Coherent), a quadruple band excitation
467 filter, a 100x oil-immersion objective (CFI Apo TIRF 100x, N.A. 1.49), two beam splitters, four
468 separate EMCCD cameras (iXon DU897, Andor), hardware focus stabilization and a
469 temperature control system. Coverslips were mounted in a microscopy chamber filled with
470 imaging buffer. The objective and the sample were maintained at 20 °C by means of a water-
471 cooled inset and objective ring connected to a thermostated water bath. Images in the four
472 channels were acquired simultaneously on the four separate EMCCD cameras. Image
473 sequences (400 frames) were taken in crop and frame-transfer mode, resulting in an acquisition
474 speed of 35 frames/s (i.e. one image every 28 ms).

475 PALM imaging was performed by TIRF microscopy immediately after the acquisition for single-
476 particle tracking. In this case, cells were additionally transfected 24 h before the experiment with
477 the photoconvertible probe mEOS-LifeAct (a kind gift of Markus Sauer, University of Würzburg,
478 Germany). mEOS was excited at 561 nm, while applying low-intensity 405 nm laser light to
479 induce photoconversion. 10,000 frames were acquired at a speed of 35 frames/s.
480 Superresolved images were then obtained using the rapidSTORM software[35].

481 Images from different channels were registered against each other using a linear piecewise
482 transformation in *Matlab* based on reference points obtained with multicolour fluorescent beads
483 (TetraSpeck; 100 nm size).

484

485 **Single particle tracking and subsequent analyses**

486 Single particle detection and tracking were performed using the u-track software[36] in Matlab
487 environment as previously described[4]. The interchannel localization precision after coordinate
488 registration by linear piecewise transformation was ~20 nm. For the analysis of receptor:G
489 protein interactions, a non-related membrane receptor (CD86) with diffusion characteristics
490 comparable to those of the α_{2A}-AR was used as negative control and as reference for random
491 colocalizations[4]. A method based on deconvolution of the observed interaction times with the
492 Lucy-Richardson algorithm[37,38] was then applied to estimate the underlying duration of
493 receptor:G protein interactions (see Supplementary Methods and Extended Data Fig. 7).

494 To investigate the motion of receptors and G proteins during or immediately before/after an

495 interaction (Fig. 3i-k and Extended Data Fig. 9c), we considered only apparent interactions with
496 duration ≥ 1.1 s, so that random colocalization represented only a small fraction (approximately
497 15%), based on a comparison between α_{2A}-AR (NE 100 μM) and CD86 (used as negative
498 control).

499 Detailed information about the computational analyses can be found in Supplementary
500 Methods.

501

502 **Hidden Markov model (HMM) analysis**

503 A software based on a variational Bayesian treatment of HMMs (vbSPT)[8] was used to identify
504 discrete diffusive states in the single molecule trajectories and analyse their characteristics. The
505 number of iterations and bootstrapping were set to 25 and 100, respectively. Diffusion
506 coefficients and dwell times derived from the analysis were used to estimate the size of the
507 corresponding nanocompartments on the plasma membrane (see Supplementary Methods).

508

509 **Spatial mapping of receptor/G protein dynamics**

510 Spatial maps of diffusivity (D) and potential energy (V) were obtained using the InferenceMAP
511 software[9], based on Bayesian inference, considering a physical model of diffusion in a potential
512 field. Only well-adhering cells with a flat plasma membrane were chosen to avoid artefacts due
513 to uneven distance from the coverslip. The flatness of the plasma membrane was verified by
514 staining with a fluorescent phospholipid (CellMask Green). The analysed areas were partitioned
515 in small regions of variable size by Voronoi tessellation[9]. The number of regions was optimized
516 to avoid areas with low number of localizations. The obtained potential energy maps were
517 subsequently used to perform particle-based stochastic simulations of receptor:G protein
518 interactions (see Supplementary Methods).

519

520 **Statistics and reproducibility**

521 Statistical analyses were performed using the Prism 6 software (GraphPad Software).
522 Differences between two groups were assessed by two-sided Student´s t-test. Differences
523 among three or more groups were assessed by one-way or two-way analysis of variance
524 (ANOVA), as appropriate, followed by Tukey's multiple comparison test (with the exception of
525 the data in Figure 3d, right, which were compared by two-sided unpaired t-test with Bonferroni

526 correction). Differences in categorical variables were assessed by chi-square test. Differences
527 were considered significant for P values < 0.05.

528

529 **Data availability**

530 The data that support the findings of this study are available from the corresponding author
531 upon reasonable request.

532

533 **Code availability**

534 Matlab scripts are available from the corresponding author upon reasonable request.

535

536 25 Lukinavicius, G. *et al.* Fluorogenic probes for live-cell imaging of the cytoskeleton. *Nat.*
537 *Methods* **11**, 731-733 (2014).

538 26 Lukinavicius, G. *et al.* A near-infrared fluorophore for live-cell super-resolution microscopy
539 of cellular proteins. *Nat. Chem.* **5**, 132-139 (2013).

540 27 Frank, M., Thumer, L., Lohse, M. J. & Bunemann, M. G Protein activation without subunit
541 dissociation depends on a $G\alpha_i$-specific region. *J. Biol. Chem.* **280**, 24584-24590 (2005).

542 28 Bahia, D. S. *et al.* Hydrophobicity of residue 351 of the G protein $G_{i1}\alpha$ determines the extent
543 of activation by the α_{2A}-adrenoceptor. *Biochemistry* **37**, 11555-11562 (1998).

544 29 Hein, P. *et al.* G_s activation is time-limiting in initiating receptor-mediated signaling. *J. Biol.*
545 *Chem.* **281**, 33345-33351 (2006).

546 30 Hoffmann, C. *et al.* A FlAsH-based FRET approach to determine G protein-coupled receptor
547 activation in living cells. *Nat. Methods* **2**, 171-176 (2005).

548 31 van Unen, J. *et al.* A New Generation of FRET Sensors for Robust Measurement of $G\alpha_{i1}$,
549 $G\alpha_{i2}$ and $G\alpha_{i3}$ Activation Kinetics in Single Cells. *PLoS One* **11**, e0146789 (2016).

550 32 Traynor, J. R. & Nahorski, S. R. Modulation by μ-opioid agonists of guanosine-5'-O-(3-
551 [35S]thio)triphosphate binding to membranes from human neuroblastoma SH-SY5Y cells.
552 *Mol. Pharmacol.* **47**, 848-854 (1995).

553 33 Vilardaga, J. P., Bünemann, M., Krasel, C., Castro, M. & Lohse, M. J. Measurement of the
554 millisecond activation switch of G protein-coupled receptors in living cells. *Nat. Biotechnol.*

555 **21**, 807-812 (2003).

556 34 Bünemann, M., Frank, M. & Lohse, M. J. G_i protein activation in intact cells involves subunit
557 rearrangement rather than dissociation. *Proc. Natl. Acad. Sci. U. S. A.* **100**, 16077-16082
558 (2003).

559 35 Wolter, S. *et al.* rapidSTORM: accurate, fast open-source software for localization
560 microscopy. *Nat. Methods* **9**, 1040-1041 (2012).

561 36 Jaqaman, K. *et al.* Robust single-particle tracking in live-cell time-lapse sequences. *Nat.*
562 *Methods* **5**, 695-702 (2008).

563 37 Richardson, W. H. Bayesian-Based Iterative Method of Image Restoration. *J. Opt. Soc. Am.*
564 **62**, 55-59 (1972).

565 38 Lucy, L. B. An iterative technique for the rectification of observed distributions. *Astron. J.* **79**,
566 745-754 (1974).

567

568 **Extended Data Figure legends**

569 **Extended Data Figure 1 | Control experiments. a-c,** Functional characterization of the
570 SNAP/CLIP tagged receptor/G protein constructs. **a**, FRET measurements of G_i protein
571 activation to test the SNAP-tagged α_{2A}-AR construct. HEK-293 cells were co-transfected with a
572 FRET sensor for G_i protein activation ($G\beta_1$-2A-cpV-$G\gamma_2$-IRES-$G\alpha_{i2}$-mTq2) and either wild-type or
573 SNAP-tagged α_{2A}-AR (n=9, 11 cells). Concentration response relationships were obtained from
574 FRET measurements in which the cells were stimulated with increasing concentrations of NE.
575 The SNAP-tagged β_2-AR construct was tested in a previous study[4]. **b**, GTPγS binding assay to
576 test the CLIP-tagged $G\alpha_i$ and $G\alpha_s$ constructs. The corresponding wild-type constructs were
577 used as control. Shown are time courses of GTPγS binding in the presence or absence of
578 agonist (left, clonidine, 10 µM; right, isoproterenol, 10 µM) (n=3 biological replicates per
579 condition). **c**, Efficiency of extracellular labelling with the cell impermeable SNAP substrate
580 S549-BG in cells transfected with CD86 carrying two SNAP tags at its N-terminus (n=28, 13, 17,
581 14 and 11 cells). **d,** Efficiency of intracellular labelling with the cell permeable CLIP substrate
582 SiR-BC in cells transfected with CD86 carrying two CLIP tags at its C-terminus (n=18, 26, 31, 27
583 cells). Labelling efficiencies in **c** and **d** were determined by fitting single-particle intensity data
584 with a mixed Gaussian model[4]. The following concentrations were chosen for subsequent
585 experiments: 4 µM S549-BG (labelling efficiency 91.1±2.9%) and 8 µM SiR-BC (labelling

586 efficiency 82.6±2.1%). **e**, Specificity of labelling. Shown are TIRF images of CHO cells
587 transfected with different combinations of SNAP-α_{2A}-AR and Gα_i-CLIP, followed by labelling with
588 S549-BG or SiR-BC (except for the positive control cotransfected with SNAP-α_{2A}-AR and Gα_i-
589 CLIP, which was labelled with both fluorescent substrates). Unspecific labelling in either mock or
590 cross-transfected cells was responsible for 2-3 spots per cell on average against ~300-400 in
591 the positive controls. This very low number of unspecific immobile localizations (<1%) does not
592 significantly interfere with the analyses of this study. **f,** Representative potential energy (*V*) maps
593 calculated in mock-transfected cells. Shown are results obtained after adding simulated
594 trajectories with Brownian motion to reproduce a condition of diffusing particles over immobile
595 unspecific localizations. The presence of immobile unspecific localizations was not sufficient to
596 generate local low potential energy areas (see **Extended Data Fig. 4b** for comparison). Data
597 are mean±s.e.m. Images (**e, f**) represent 3 independent experiments.

598

599 **Extended Data Figure 2 | MSD analysis of receptor and G protein trajectories. a,** Scatter
600 plot of diffusion coefficient (*D)* and anomalous diffusion exponent (α) values estimated for
601 simulated trajectories with Brownian motion and characteristics similar to those of α_{2A}-ARs. The
602 results were used to set the cut-offs for classifying the trajectories into four groups according to
603 their motion: immobile (D<0.01 μm^2 s^{-1}), sub-diffusion (α<0.75), normal diffusion (0.75≤α≤1.25)
604 and super-diffusion (α>1.25). **b,** Scatter plot as in **a** for α_{2A}-AR trajectories. **c,** Representative
605 α_{2A}-AR and Gα_i trajectories classified in the four groups. **d**, Relative frequency distributions of
606 the trajectories in the four groups (left) and corresponding *D* values (right) for receptors and G
607 proteins under basal and stimulated conditions. The control CD86 was expressed together with
608 wild-type α_{2A}-AR and stimulated with NE to verify if the effects observed upon agonist
609 stimulation were specific for Gα_i. Differences in **d** are statistically significant by two-way ANOVA.
610 #, P<0.05, ##, P<0.01 and ####, P<0.0001 vs. the corresponding basal condition and **,
611 P<0.01, ***, P<0.001, ****, P<0.0001, vs. α_{2A}-AR basal (top) or β_2-AR basal (bottom) by Tukey's
612 multiple comparison test. Data are mean±s.e.m. n=30 (9,273), 17 (6,623), 37 (8,309), 30
613 (4,699), 18 (2,182), 36 (5,240), 28 (11,267), 27 (12,697), 29 (10,760), 47 (16,461), 29 (41,079)
614 and 47 (7,585) cells (trajectories) for α_{2A}-AR basal, α_{2A}-AR NE, α_{2A}-AR UK-14,304, Gα_i basal,
615 Gα_i NE, Gα_i UK-14,304, CD86 basal, CD86 NE, β_2-AR basal, β_2-AR Iso, Gα_s basal, Gα_s Iso,
616 respectively. Images (**c**) represent 5 independent experiments.

617

618 **Extended Data Figure 3 | Complete results of the hidden Markov model (HMM) analysis.**
619 Differences are statistically significant by two-way ANOVA. #, P<0.05, ##, P<0.01, ###, P<0.001
620 and ####, P<0.0001 vs. the corresponding basal condition, and *, P<0.05, **,P<0.01, ***,
621 P<0.001 and ****: P<0.0001 vs. α_{2A}-AR basal (for $G\alpha_i$ and CD86) or β_2-AR basal (for $G\alpha_s$) by
622 Tukey's multiple comparison test. Data are mean±s.d. n=22 (85,475), 11 (44,797), 31 (153,072),
623 13 (47,062), 9 (15,161), 30 (88,397), 28 (110,907), 30 (147,222), 27 (142,243), 44 (229,815), 28
624 (84,668) and 44 (171,623) cells (trajectories) for α_{2A}-AR basal, α_{2A}-AR NE, α_{2A}-AR UK-14,304,
625 $G\alpha_i$ basal, $G\alpha_i$ NE, $G\alpha_i$ UK-14,304, CD86 basal, CD86 NE, β_2-AR basal, β_2-AR Iso, $G\alpha_s$ basal,
626 $G\alpha_s$ Iso, respectively. N.D., not determinable.

627

628 **Extended Data Figure 4 | Complex diffusion dynamics of α_{2A}-AR and $G\alpha_i$. a,** density maps
629 of α_{2A}-AR and $G\alpha_i$ localizations (selected trajectories overlaid in different colours; arrowheads,
630 areas of high density). **b**, Potential energy (*V*) maps for α_{2A}-AR and $G\alpha_i$, calculated for the same
631 membrane region. **c,** Merge of potential energy maps in **b** (top) and line-profile plot along the
632 dashed line (bottom). Arrowheads, hot spots where *V* is low for both α_{2A}-AR and $G\alpha_i$. **d**,
633 Additional examples of α_{2A}-AR potential energy (*V*) maps over actin PALM images and
634 corresponding zoom-in views. Images represent 3 (**a**-**c**) and 2 (**d**) independent experiments.

635

636 **Extended Data Figure 5 | Complex diffusion dynamics of β_2-AR and $G\alpha_s$. a,** β_{2A}-AR
637 localizations over $G\alpha_s$ potential energy (*V*) map and vice versa (top) and quantifications of
638 relative potential energy at the localizations ($V_{L,rel}$; bottom). A negative value indicates relatively
639 lower potential energy at the localizations. **b**, β_2-AR:$G\alpha_s$ interactions over merged β_2-AR and
640 $G\alpha_s$ potential energy map (top) and corresponding quantifications (bottom). Arrowheads,
641 localizations concentrated at hot spots. **c-e,** β_2-AR trajectories over images of tubulin (**c**), actin
642 (**d**) or CCPs (**e**) (top) and corresponding colocalization analyses (bottom). Negative
643 colocalization index (*I*) values indicate preferential avoidance of the imaged structures by the
644 receptors. **f,** Trajectory of β_2-AR stopping at CCP (arrowhead; top) and corresponding
645 quantitative analysis (bottom). The trajectory is colour-coded according to the HMM states.
646 Results in **a-e** were compared to those obtained with random localizations. See Supplementary
647 Methods for details. Data are mean±s.d. n, number of cells. #, P<0.05, ##, P<0.01, ###,
648 P<0.001, ####, P<0.0001 vs. random localizations by two-sided paired t-test. *, P<0.05, **,
649 P<0.01, ***, P<0.001, ****, P<0.0001 vs. β_2-AR (basal) by two-sided unpaired t-test.

650

651 **Extended Data Figure 6 | Complex diffusion dynamics of Gα_i. a**, Gα_i trajectories over actin
652 PALM image. Arrowheads, Gα_i subunits crossing over actin fibres. **b,** Gα_i trajectories over
653 image of CCPs. **c,** Gα_i potential energy (*V*) map over PALM image of actin fibres (left) and
654 corresponding zoom-in view (right). Images represent 2 (**a**, **c**) and 3 (**b**) independent
655 experiments.

656

657 **Extended Data Figure 7 | Validation of the analysis of receptor:G protein interactions**
658 **using simulated data. a-d,** Test of the Lucy-Richardson (LR) deconvolution algorithm on data
659 obtained with numerical simulations. A numerical simulation of particles interacting and
660 dissociating following an exponential law (n=20,000 particles; k_{off}=0.7 s^{-1}) was performed. In
661 addition, we considered particles undergoing random colocalizations (also terminating following
662 an exponential law; n=20,000 particles; k=1.75 s^{-1}). **a,** Underlying distribution of the interaction
663 times for the true interactions. **b,** Distribution of the colocalization times for the random
664 colocalizations. **c,** Convolution of the distribution in **a** with that in **b**, corresponding to the
665 observed colocalization times. **d,** Deconvolution of the distribution in **c** with that in **b**. Note that
666 the algorithm was capable of correctly retrieving the distribution of the true interaction times. **e,**
667 **f,** Simulated two-channel image sequences of particles undergoing transient interactions. A
668 defined fraction of particles in the first channel was simulated to undergo interactions with
669 particles in the second channel. The synthetic image sequences were then analysed using
670 automated particle detection and tracking as for the experimental ones. **e,** Representative frame
671 of a simulated two-colour image sequence. **f,** Trajectories obtained by automated single-particle
672 detection and tracking. **g,** Relaxation curve obtained from simulations of non-interacting
673 particles. **h,** Relaxation curve obtained from simulations of interacting and non-dissociating
674 particles. **i,** Result of the LR deconvolution analysis of the data in **h** with those in **g**. Data were
675 fitted with an exponential decay, used to estimate the rate of premature termination (see
676 Supplementary Methods). **j**, Results of the LR deconvolution analysis on simulated image
677 sequences comparing the input dissociation rate constants (k_{off}) and the ones estimated by the
678 analysis. The results were corrected for premature termination of the interactions as described
679 in Supplementary Methods. All simulations were repeated 3 times with similar results.

680

681 **Extended Data Figure 8 | Simulations with deterministic model of GPCR signalling. a,**

682 Schematic representation of the model. r, inactive receptor. R, active receptor. L, ligand
683 (agonist). **b,** Model reactions and kinetics parameters used in the simulations. **c, d,** FRET
684 measurements of the ensemble kinetics of α_{2A}-AR activation/deactivation in response to
685 transient agonist stimulation. A sensor consisting in the α_{2A}-AR carrying a FlAsH tag in the third
686 intracellular loop and CFP at the C-terminus was used. Shown are a representative FRET
687 measurement (**c**) and the normalized average of the FRET data (**d**; n=4 cells). **e,** Fitting of
688 model parameters using the measured FRET data for receptor activation/deactivation. **f,**
689 Concentration-response relationships for ligand binding, receptor activation and G protein
690 activation generated with the model. **g, h,** Simulations of GPCR signalling in response to
691 transient agonist stimulation, applying the estimated k_{on} and k_{off} for receptor:G protein
692 interactions to the model. Simulations were performed both considering low (**g**) and high (**h**)
693 receptor/G protein expression levels. **i, j,** FRET measurements of the ensemble kinetics of α_{2A}-
694 AR:Gα_i association/dissociation in response to transient agonist stimulation. A sensor consisting
695 in the α_{2A}-AR carrying YFP at the C-terminus and the Gα_{i1} subunit carrying CFP in the αA-αB
696 loop within the α-helical domain was used. Shown are a representative FRET measurement (**i**)
697 and the normalized average (n=16 cells) of the FRET data (**j**). Association and dissociation time
698 constants (mean, 95%CI) were 44.4 (38.3-52.9) ms and 1.22 (1.16-1.29) s. **k,** Comparison
699 between the FRET data in **j** and the result of simulation with the mathematical model. Data are
700 mean±s.e.m.

701

702 **Extended Data Figure 9 | Hot spots for receptor:G protein interaction in primary human**
703 **endothelial cells. a,** α_{2A}-AR:Gα_i interactions over merged α_{2A}-AR and Gα_i potential energy (V)
704 map (left) and corresponding quantifications (right). Arrowheads, α_{2A}-AR:Gα_i interactions
705 concentrated at hot spots. **b**, Same analysis as in **a** for β_2-AR and Gα_s. ####, P<0.0001 vs.
706 random localizations by two-sided paired t-test. **c**, Distribution of diffusion states (based on
707 HMM analysis) of receptor/G protein trajectories during apparent interactions. Differences are
708 statistically significant by chi-square test (****, P<0.0001; n=2,488,438 and 1,382,193 data
709 points for α_{2A}-AR and Gα_i with NE stimulation; n=1,992,190 and 874,317 data points for α_{2A}-AR
710 and Gα_i with UK-14,304 stimulation; n=5,073,163 and 3,959,938 data points for β_2-AR and Gα_s
711 with Iso stimulation, respectively). Data (**a**, **b**) are mean±s.d. n, number of cells (**a**, **b**).

712

713 **Extended Data Figure 10 | Schematic summary. a,** The complex organization of the plasma

714 membrane, including barriers provided by actin fibres, microtubules and CCPs, generates hot
715 spots for receptor:G protein interaction and signalling. **b,** Receptors and G proteins undergo
716 random collisions (preferentially within these hot spots), which, via very short-lived encounter
717 complexes, only seldom lead to the formation of productive receptor:G protein (R:G) complexes
718 (low k_{on}). Most of these complexes dissociate with a lifetime of ~1-2 s, while very few are long-
719 lived. Agonists mainly act by increasing the k_{on} for receptor:G protein interactions in a ligand-
720 specific manner. These data suggest that most receptor:G protein complexes are transient and
721 that receptor:G protein interactions are not diffusion limited but rather controlled by the large
722 conformational rearrangements occurring during the formation of productive receptor:G protein
723 complexes. See also Supplementary Discussion.

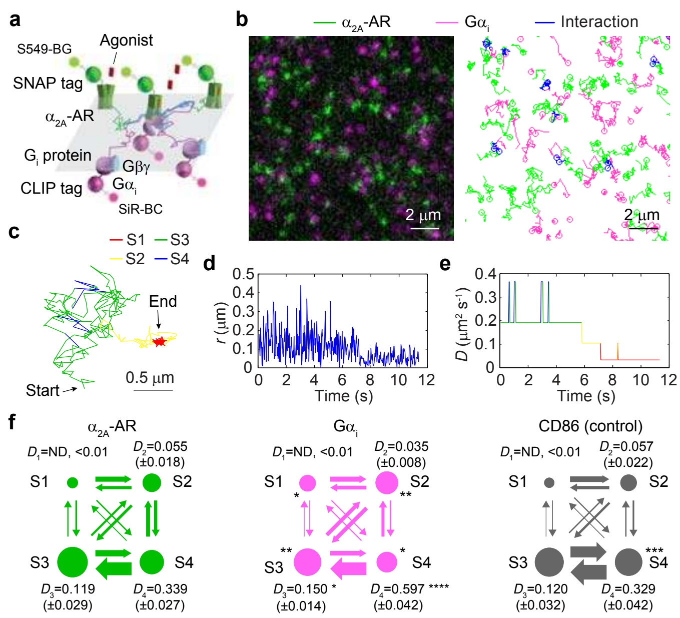
a
b
c
d
e
f
Agonist
S549-BG
SNAP tag
α2A-AR
Gi protein
Gβγ
CLIP tag
Gαi
SiR-BC
α2A-AR
Gαi
Interaction
2 μm
2 μm
S1
S2
S3
S4
End
Start
0.5 μm
r (μm)
Time (s)
D (μm² s⁻¹)
Time (s)
α2A-AR
Gαi
CD86 (control)
D1=ND, <0.01
D2=0.055 (±0.018)
D3=0.119 (±0.029)
D4=0.339 (±0.027)
D1=ND, <0.01
D2=0.035 (±0.008)
D3=0.150 * (±0.014)
D4=0.597 **** (±0.042)
D1=ND, <0.01
D2=0.057 (±0.022)
D3=0.120 (±0.032)
D4=0.329 (±0.042)

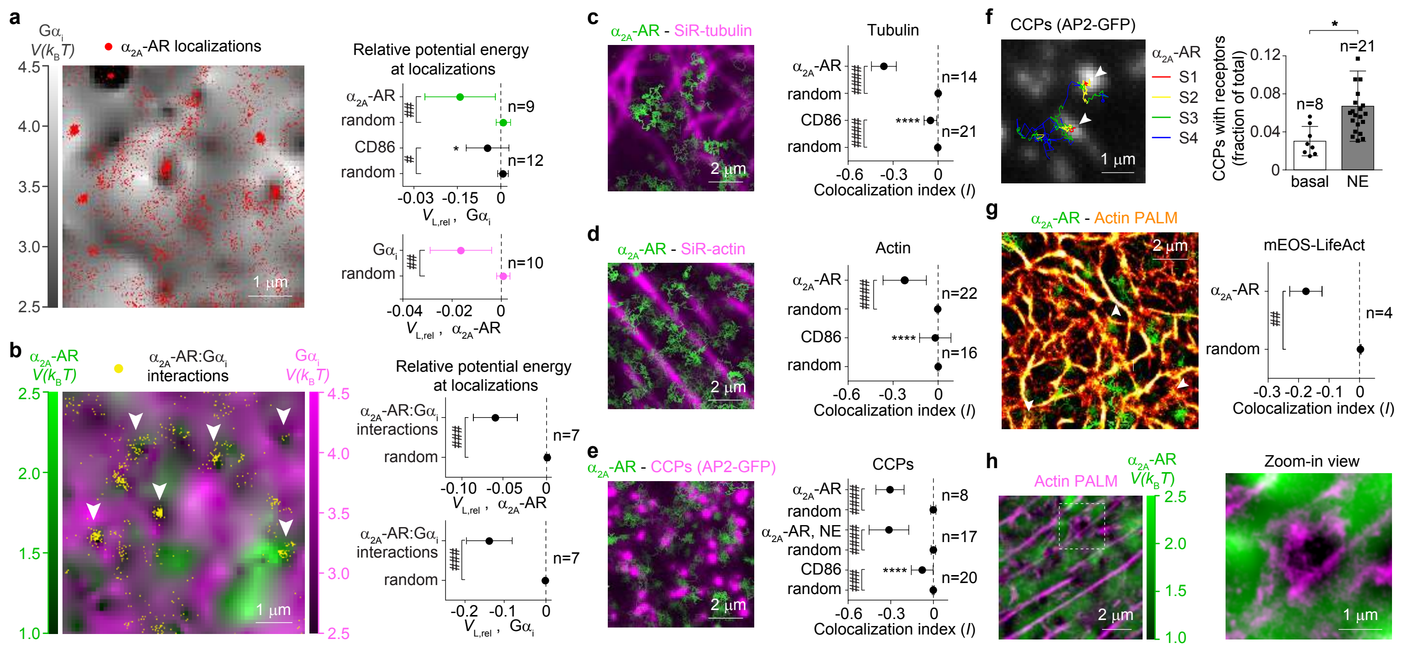

a
Gα$_i$ V(k_BT)
α$_{2A}$-AR localizations
1 μm
Relative potential energy at localizations
α$_{2A}$-AR
random
CD86
random
n=9
n=12
Gα$_i$
random
n=10
b
α$_{2A}$-AR V(k_BT)
α$_{2A}$-AR:Gα$_i$ interactions
Gα$_i$ V(k_BT)
Relative potential energy at localizations
α$_{2A}$-AR:Gα$_i$ interactions
random
n=7
c
α$_{2A}$-AR - SiR-tubulin
Tubulin
n=14
n=21
Colocalization index (I)
d
α$_{2A}$-AR - SiR-actin
Actin
n=22
n=16
e
α$_{2A}$-AR - CCPs (AP2-GFP)
CCPs
α$_{2A}$-AR, NE
n=8
n=17
n=20
2 μm
f
CCPs (AP2-GFP)
S1
S2
S3
S4
CCPs with receptors (fraction of total)
basal
NE
g
α$_{2A}$-AR - Actin PALM
mEOS-LifeAct
n=4
h
Actin PALM
Zoom-in view

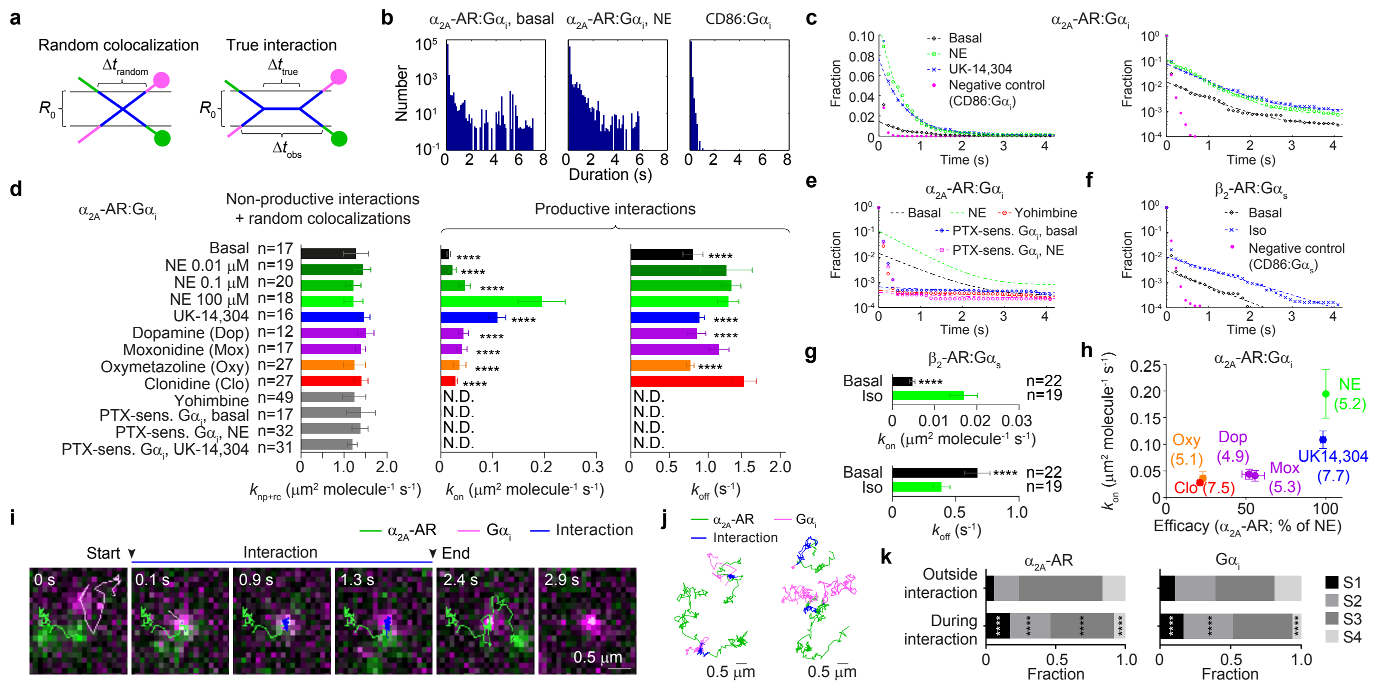

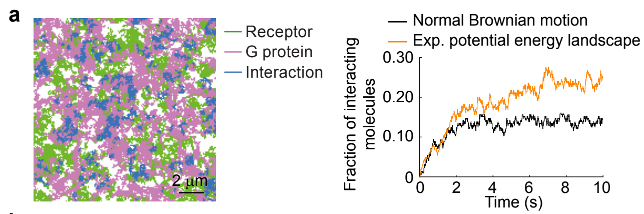
a
Receptor
G protein
Interaction
2 µm
Normal Brownian motion
Exp. potential energy landscape
Fraction of interacting molecules
0.30
0.20
0.10
0
0
2
4
6
8
10
Time (s)

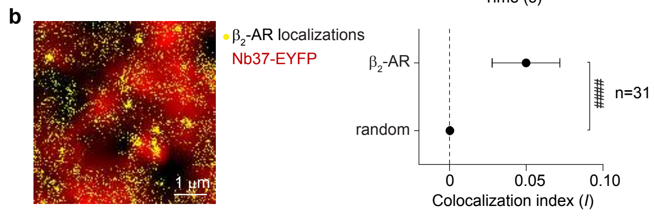
b
β2-AR localizations
Nb37-EYFP
1 µm
β2-AR
random
n=31
0
0.05
0.10
Colocalization index (I)